

Observational Evidence of the Salient Features of the Universe

EKATERINA S. IVSHINA¹

¹*Department of Mathematics, Princeton University, Princeton, NJ 08544, USA*

Contents

1. Homogeneity and Isotropy of the Universe	1
1.1. Isotropy	1
1.2. Homogeneity	2
2. Expansion and Evolution of the Universe	4
3. Spatially Flat Universe	5
4. Existence of Thermal Radiation Background and its Anisotropy	6
5. Chemical Composition of the Universe	8
6. More Baryonic Matter Than Antimatter	10
7. Hierarchy of Gravitationally Bound structure: Bottom to Top	12
8. Ordinary Matter = 1/5 All Matter	13
9. Existence of Super-massive Black Holes	13
10. Total Mass Energy = 30 % of Total Energy	14
11. Entropy	15
12. Vacuum May Be Metastable or Unstable	16
1. HOMOGENEITY AND ISOTROPY OF THE UNIVERSE	
1.1. <i>Isotropy</i>	

Cosmological homogeneity and isotropy, i.e., the Cosmological Principle, is a fundamental assumption in modern Cosmology (see, e.g., Goodman (1995); Clarkson & Maartens (2010)). We may probe the isotropy of the Universe as follows: using the

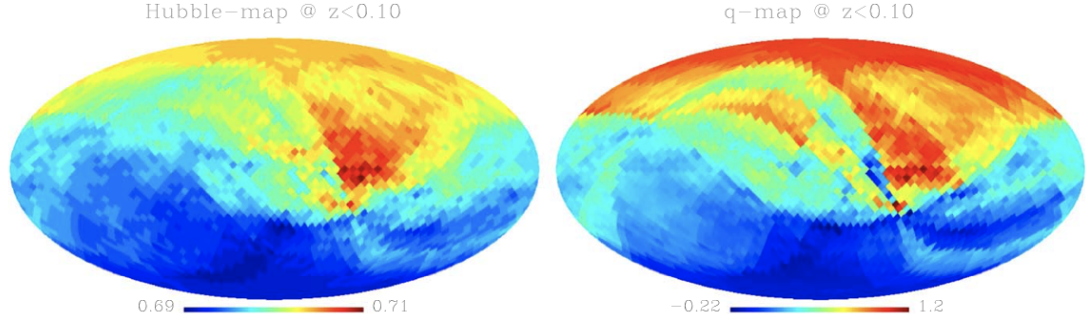


Figure 1. Hubble-map of Pantheon SNe at $z \leq 0.10$ (left panel), and the q -map at the same redshift range (right panel). Source: [Andrade et al. \(2018\)](#).

angular dependence of the Type Ia Super-novae (SN Ia) Hubble diagram, one can compare the variation of the best-fit cosmological parameters across the sky with the synthetic data sets based on the concordance model, or idealized sky distribution of data points. [Andrade et al. \(2018\)](#) used Super Novae dataset containing 1049 objects lying in the interval $0.01 < z < 2.30$ taken from the PanSTARRS1 Medium Deep Survey, SDSS, SNLS, in addition to many low- z and HST data points. To perform the isotropy test in a model-independent way, [Andrade et al. \(2018\)](#) used a cosmographic approach ([Visser 2004](#)) focusing on a low- z range: they selected objects at $z \leq 0.10$ and $z \leq 0.20$, reducing the sample to 211 and 411 data points, respectively.

[Andrade et al. \(2018\)](#) quantifies the anisotropy by defining $\Delta p = p_0^{\max} - p_0^{\min}$ where p_0^{\max} and p_0^{\min} are, respectively, the maximum and minimum best fits for $p \rightarrow h_0$ or q_0 obtained across the entire celestial sphere, h_0 is the dimensionless Hubble constant, and q_0 is the decelerating parameter at present time. The authors showed the Hubble-maps for both $z \leq 0.10$ and $z \leq 0.20$ in the left panels of Figures 1 and 2, respectively. In the right subplots of the same figures, they show the q -maps in the same red-shift intervals.

The resulting anisotropy estimates are summarized in Table 3. Allowing for the $1-\sigma$ error-bars in both h_{\max} and h_{\min} values, [Andrade et al. \(2018\)](#) obtained $\Delta h = 0.026 \pm 0.086$ ($z \leq 0.10$) and $\Delta h = 0.024 \pm 0.058$ ($z \leq 0.20$), which is compatible with the h_0 uncertainty due to cosmic variance ([Camarena & Marra 2018](#)). The authors note that the regions of highest h_0 coincide with those hemispheres with the lowest SN Ia counts, which may indicate a bias in both hubble- and q -maps due to it. Finally, [Andrade et al. \(2018\)](#) conclude that there is null evidence against the cosmological principle in the low-redshift universe.

1.2. Homogeneity

Recent measurements of cosmic homogeneity were performed in [Ntelis et al. \(2017\)](#) and [Gonçalves et al. \(2018\)](#). Below we discuss in detail the work performed in [Ntelis et al. \(2017\)](#).

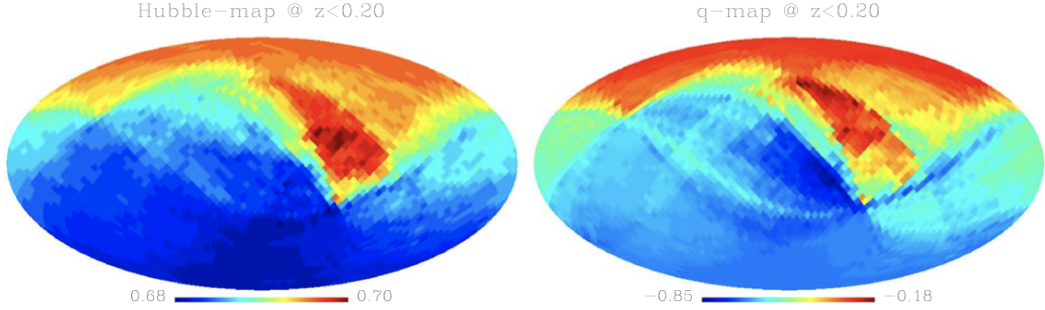


Figure 2. Hubble-map of Pantheon SNe at $z \leq 0.20$ (left panel), and the q -map at the same redshift range (right panel). Source: [Andrade et al. \(2018\)](#)

Hubble-map			
z Range	Δh	<i>MC-iso</i> p-value (%)	<i>MC-lcdm</i> p-value (%)
$z \leq 0.10$	0.026	0.3	7.3
$z \leq 0.20$	0.024	< 0.1	7.1
<i>q</i> -map			
z Range	Δq	<i>MC-iso</i> p-value (%)	<i>MC-lcdm</i> p-value (%)
$z \leq 0.10$	1.440	37.4	47.9
$z \leq 0.20$	0.670	0.1	12.5

Figure 3. The redshift range, Δh , and the p -values for each MC data set for the Hubble-map and q -map. Source: [Andrade et al. \(2018\)](#)

Ntelis et al. (2017) used the data release 12 of BOSS CMASS galaxy sample, which is a survey that allows to study the 3D distribution of $\sim 1.4 \times 10^6$ galaxies and $\sim 10^5$ quasars and their Lyman- α forests within an effective area of $\sim 10,000 \text{ deg}^2$. To study the evolution of the clustering of the CMASS galaxy sample, the authors divided their data sample into 5 redshift intervals, as defined in table 4. Ntelis et al. (2017) then converted the redshift measurements to comoving distances assuming a flat ΛCDM model with parameters defined in equation (1.1) in their paper. In the end, the sample has a total effective volume of $3.8 \text{ h}^{-3} \text{ Gpc}^3$.

To test for homogeneity, the authors used the counts-in-spheres, $N(< r)$, i.e. the average number of objects around a given object, and its logarithmic derivative, the fractal correlation dimension, $D_2(r)$. For a homogeneous sample, we expect to have $N(< r) \propto r^3$ and $D_2 = 3$. Ntelis et al. (2017) define a characteristic homogeneity scale, R_H , as the value for which D_2 reaches the homogeneous value within 1%, i.e. $D_2(R_H) = 2.97$. The authors obtained $3 - \langle D_2 \rangle = (0.6 \pm 1.3) \times 10^{-3}$ at $1-\sigma$ over the range $300h^{-1} \leq r \leq 1300h^{-1} \text{ Mpc}$, consistent with homogeneity, and a transition to homogeneity at $R_H = 114.2 \pm 5.8h^{-1} \text{ Mpc}$. Ntelis et al. (2017) note that with their

z	NGC	SGC
0.430–0.484	101,383	40,170
0.484–0.538	174,468	63,518
0.538–0.592	151,084	56,805
0.592–0.646	97,155	37,179
0.646–0.700	47,289	17,899
0.430–0.700	571,379	215,571

Figure 4. DR12 data sample in 5 redshift intervals in north (NGC) and south (SGC) galactic caps. Source: [Ntelis et al. \(2017\)](#).

dataset, they can not test for a possible isotropic variation of the density with redshift, $\rho = \rho(z)$. In other words, they can only check for spatial isotropy, $\rho(z, \theta_1) = \rho(z, \theta_2)$. Assuming the Copernican principle the data in this study imply homogeneity of the galaxy sample without any Λ CDM assumption. Due to the large cosmic depth of the BOSS survey, the authors were able to study the redshift evolution of the transition to homogeneity scale and found agreement with the Λ CDM prediction.

2. EXPANSION AND EVOLUTION OF THE UNIVERSE

In 1929, Edwin Hubble published a paper reporting observational evidence suggesting that the Universe is expanding ([Hubble 1929](#)). Nowadays, tensions remain in the estimates of the Hubble constant H_0 derived through different methods. [Aghanim et al. \(2020\)](#) reports $H_0 = 67.27 \pm 0.6 \text{ km s}^{-1} \text{ Mpc}^{-1}$ (68 %, TT, TE, EE + lowE), a value derived using *Planck* data and assuming the base- Λ CDM cosmology with minimal neutrino mass. [Aghanim et al. \(2020\)](#) defines the base- Λ CDM cosmology as the standard spatially-flat 6-parameter Λ CDM cosmology having a power-law spectrum of adiabatic scalar perturbation. Including CMB lensing, the authors place a sharper constraint on the Hubble constant: $H_0 = 67.36 \pm 0.54 \text{ km s}^{-1} \text{ Mpc}^{-1}$ (68 %, TT, TE, EE + lowE+lensing). [Aghanim et al. \(2020\)](#) call the above value their “best estimate” of H_0 from *Planck*, assuming the base- Λ CDM cosmology.

In the SH0ES21 project, [Riess et al. \(2011\)](#) provides a distance-ladder estimate of the Hubble constant: $H_0 = (73.8 \pm 2.4) \text{ km s}^{-1} \text{ Mpc}^{-1}$. After acquiring new parallax measurements of 7 long-period (> 10 days) Milky Way Cepheids using astrometry from spatial scanning of WFC3 on HST, [Riess et al. \(2018\)](#) concluded that $H_0 = 73.48 \pm 1.66 \text{ km s}^{-1} \text{ Mpc}^{-1}$, which exacerbates the tension with the *Planck* results. Using Gaia parallaxes, [Riess et al. \(2018\)](#) slightly improved their constraint to $H_0 = 73.52 \pm 1.62 \text{ km s}^{-1} \text{ Mpc}^{-1}$. Recently, [Riess et al. \(2019\)](#) used updated measurements of LMC Cepheids and estimated $H_0 = 74.03 \pm 1.42 \text{ km s}^{-1} \text{ Mpc}^{-1}$. It is possible

that the discrepancy between the results is due to yet unidentified systematic errors in the Planck or SH0ES data (see, e.g., Spergel et al. (2015); Addison et al. (2016); and N. Aghanim et al. (2017)).

Hagstotz et al. (2022) used Fast Radio Bursts (FRBs), which are very short and bright transients visible over extragalactic distances, to measure the Hubble constant. The radio pulse signal gets dispersed along the line of sight by free electrons, most of which are associated with the large-scale structure (LSS). The total dispersion measure provides a distance estimate to the source. Hagstotz et al. (2022) used a sample of nine currently available FRBs to place a constraint on the Hubble constant: $H_0 = 62.3 \pm 9.1 \text{ km s}^{-1} \text{ Mpc}^{-1}$, where the error bar includes the uncertainty stemming from the LSS, host halo and Milky Way contributions to the observed dispersion measure.

Khetan et al. (2021) estimated the Hubble constant using Type Ia supernovae calibrated with surface brightness fluctuations (SBF) method. Having built a sample consisting of 24 SNe hosted in galaxies that have SBF distance measurements, the authors applied a hierarchical Bayesian approach to conclude $H_0 = 70.50 \pm 2.37(\text{stat}) \pm 3.38(\text{sys}) \text{ km s}^{-1} \text{ Mpc}^{-1}$.

Domínguez et al. (2019) presented a novel strategy for measuring H_0 , which is independent and complementary to the strategies based on the distance ladder, cosmic microwave background (CMB), clustering with weak lensing, and strong lensing data. This methodology relies on the observation that the extragalactic background light supplies opacity for very high energy photons via photon–photon interaction. The amount of γ -ray attenuation along the line of sight depends on the expansion rate and matter content of the universe. Using the latest γ -ray attenuation results from Fermi-LAT and Cherenkov telescopes, the authors concluded $H_0 = 67.4 \pm 6.2 \text{ km s}^{-1} \text{ Mpc}^{-1}$.

3. SPATIALLY FLAT UNIVERSE

A precise measurement of the curvature of the Universe is key for cosmology since it could not only confirm the paradigm of primordial inflation but also help in discriminating between different early-Universe scenarios. Recent observations show tensions that allow a few percent deviations from a flat universe. The base- Λ CDM model assumes that the Universe is flat. Aghanim et al. (2020) combined the Planck temperature and polarization power spectra to estimate the spatial curvature Ω_K :

$$\Omega_K = -0.056 \pm 0.028 \text{ (68 \%}, \text{ Planck TT+lowE}),$$

$$\Omega_K = -0.044 \pm 0.018 \text{ (68 \%}, \text{ Planck TT, TE, EE+lowE}),$$

which is an apparent apparent 2σ detection of curvature.

Combining with the lensing reconstruction, Aghanim et al. (2020) computed

$\Omega_K = -0.0106 \pm 0.0065 \text{ (68 \%}, \text{ TT, TE, EE+lowE+lensing)}$, a result that is consistent with a spatially flat universe at well over 2σ .

Combining the Planck data with BAO data, Aghanim et al. (2020) computed

$$\Omega_K = 0.0007 \pm 0.0019 \text{ (68 \% , TT, TE, EE+lowE+lensing+BAO).}$$

[Aghanim et al. \(2020\)](#) concluded that our Universe is spatially flat to a $1-\sigma$ based on the joint results.

[Di Valentino et al. \(2021\)](#) show that a combined analysis of cosmic microwave background anisotropy power spectra obtained by the Planck satellite and luminosity distance data simultaneously excludes a flat universe and a cosmological constant at 99% confidence level. These results hold separately when combining Planck with three different data sets: the two determinations of the Hubble constant from [Riess et al. \(2019\)](#) and [Freedman et al. \(2020\)](#), and the Pantheon catalog of high-redshift Type Ia supernovae ([Scolnic et al. 2018](#)).

[Chudaykin et al. \(2021\)](#) presented a joint analysis of the full-shape, baryon acoustic oscillations (BAO), big bang nucleosynthesis (BBN) and supernovae data. The authors found $\Omega_K = -0.043 \pm 0.036$ (68% C.L.), which is a CMB-independent constraint.

[Vagnozzi et al. \(2021\)](#) developed a dataset of cosmic chronometers (CC), i.e. measurements of the expansion rate $H(z)$ from the relative ages of massive early-type passively evolving galaxies. CC has an advantage of being virtually free of cosmological model assumptions. Combining Planck 2018 CMB temperature and polarization data with the latest CC measurements, the authors found $\Omega_K = 0.0054 \pm 0.0055$, consistent with a spatially flat Universe.

The tension in the results calls for new observations.

4. EXISTENCE OF THERMAL RADIATION BACKGROUND AND ITS ANISOTROPY

[Penzias & Wilson \(1965\)](#) discovered the CMB by measuring excess antenna temperature. The authors detected an excess of about 3.5K while measuring effective zenith noise temperature of the 20-foot horn reflector antenna at the Crawford Hill Laboratory, Holmdel, New Jersey, at 4080 Mc/s. Within the observational limits, the excess temperature was isotropic, unpolarized and did not depend on the season. The authors were aware of the work by [Dicke et al. \(1965\)](#) and supposed that relic radiation from a hotter denser early Universe may explain their measurement. Assuming that the universe was in a high-temperature state during its early stages, [Dicke et al. \(1965\)](#) showed that as the universe expands, the cosmological redshift would result in adiabatic cooling of the radiation, while preserving the thermal character. The radiation temperature would vary inversely as the expansion parameter (radius) of the universe.

The temperature measurement in [Penzias & Wilson \(1965\)](#) has been performed as follows. The authors used a radiometer that employs a traveling-wave master, a low-loss (0.027-db) comparison switch, and a liquid helium-cooled reference termination. [Penzias & Wilson \(1965\)](#) collected measurements by switching manually between antenna input and the reference termination. The antenna, reference termination,

and radiometer were well matched so that a round-trip return loss of more than 55 db existed throughout the measurement; hence errors in the measurement of the effective temperature due to impedance mismatch can be neglected. The estimated error in the measurement value of the total antenna temperature is 0.3K, which comes largely from uncertainty in the absolute calibration of the reference termination. The contribution to the antenna temperature due to atmospheric absorption, which was estimated to be 2.3 ± 0.3 K, was obtained by recording variation in antenna temperature with elevation angle and employing the secant law. The contribution to the antenna temperature from ohmic losses was calculated to be 0.8 ± 0.4 K. The backlobe response to ground radiation is taken to be less than 0.1K. From the above considerations, the authors computed that the excess temperature of antenna is 3.5 ± 1 K at 4080 Mc/s.

More recently, with increasing precision, astronomers conducted CMB observations from microwave telescopes carried by balloons and spacecraft ([Hu & White 2004](#)). In 1990, Cosmic Background Explorer (COBE, [Boggess et al. \(1992\)](#)) satellite measured the spectrum of the CMB radiation. Moreover, COBE has detected slight variations in the temperature of the CMB across the sky, with changes at the level of one part in 100,000. To map the temperature variations of the CMB, scientists have launched the Wilkinson Microwave Anisotropy Probe (WMAP) in 2001. This satellite goes around the sun in an orbit 1.5 million kilometers beyond Earth's. WAMP results showed that the hot and cold spots in the radiation fall into characteristic sizes. Having analyzed the data from the FIRAS (Far InfraRed Absolute Spectrophotometer) on board the COBE, [Fixsen et al. \(1996\)](#) refined the absolute temperature of the CMB to 2.728 ± 0.004 K and have shown that the RMS deviations from a blackbody spectrum are less than 50 parts per million of the peak of the Cosmic Microwave Background Radiation. [Fixsen et al. \(1997\)](#) studied the CMB anisotropy data from the independent COBE FIRAS and DMR observations and concluded that the mean FIRAS spectrum of the anisotropy observed by DMR is consistent with the Planck form, $\partial B / \partial T$, expected of CMB anisotropy. Conversely, the spatial distribution of the FIRAS data fit to a Planck spectrum agreed well with the DMR anisotropy. Taken together, these results provide direct observational support for the widely held view that the signal first detected by the DMR is temperature anisotropy in the CMB.

The most recent measurements of the CMB temperature and its fluctuations have been performed by [Aghanim et al. \(2020\)](#), who presented cosmological parameter results from the final full-mission Planck measurements of the cosmic microwave background (CMB) anisotropies, combining information from the temperature and polarization maps and the lensing reconstruction. The European Space Agency's Planck satellite, which was dedicated to studying the early Universe and its subsequent evolution, was launched on 14 May 2009. It scanned the microwave and submillimetre sky continuously between 12 August 2009 and 23 October 2013, producing deep, high-resolution, all-sky maps in nine frequency bands from 30 to 857GHz. Figure 5 shows the Cosmic Microwave Background observed by Planck. Figure 6 shows the

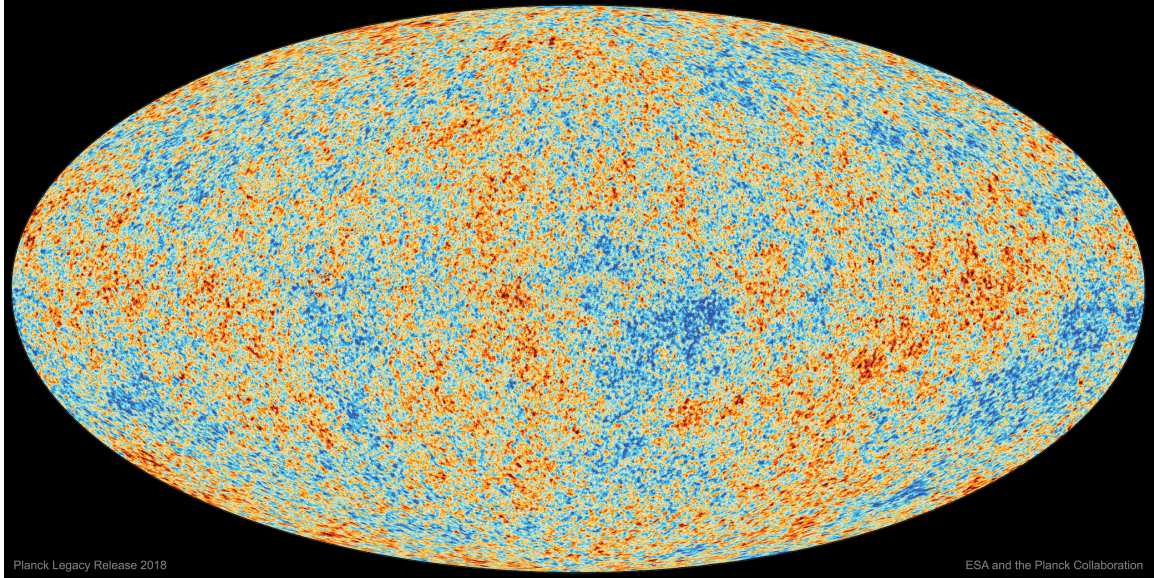


Figure 5. The Cosmic Microwave Background observed by Planck. Source: [Aghanim et al. \(2020\)](#)

angular power spectrum of the CMB. Figure 7 shows the constraints on parameters from the base- Λ CDM model derived in [Aghanim et al. \(2020\)](#).

5. CHEMICAL COMPOSITION OF THE UNIVERSE

Big bang nucleosynthesis (BBN) – a period in the evolution of the Universe during which the temperature was low enough for nuclei with mass number $A > 1$ to exist and still high enough for thermonuclear reactions to occur – is thought to be the main source of deuterium (D), helium (^3He , ^4He) and lithium (mainly ^7Li) in the universe (Steigman 2010). H and ^4He , make up the vast majority of all nuclei in the universe (Tayler 1967). A common way to determine the primordial helium abundance Y_P is to use observations of metal-poor H II regions found in blue compact dwarf galaxies. Using a spectroscopic sample of 100 H II regions collected from the Sloan Digital Sky Survey and the HeBCD database from Izotov et al. (2007), Kurichin et al. (2021) determined the primordial helium abundance to be $Y_P = 0.2462 \pm 0.0022$, which is consistent with the result from Planck survey $Y_P^{Planck} = 0.2471 \pm 0.0003$ (Aghanim et al. 2020).

There has been progress related to constraining deuterium abundance since the work produced by [Planck Collaboration et al. \(2016\)](#). On the observational side, [Cooke et al. \(2018\)](#) have published a new estimate based on their best seven measurements in metal-poor damped Ly α systems, $y_{DP} = 10^5 n_D/n_H = 2.527 \pm 0.030$ (68% CL). On the theoretical side, the value of the nuclear reaction rate $d(p, \gamma)^3\text{He}$, which impacts BBN computations of the primordial deuterium calculation, has been calculated ab initio. [Aghanim et al. \(2020\)](#) compares the results obtained when the deuterium fraction is computed in three different ways:

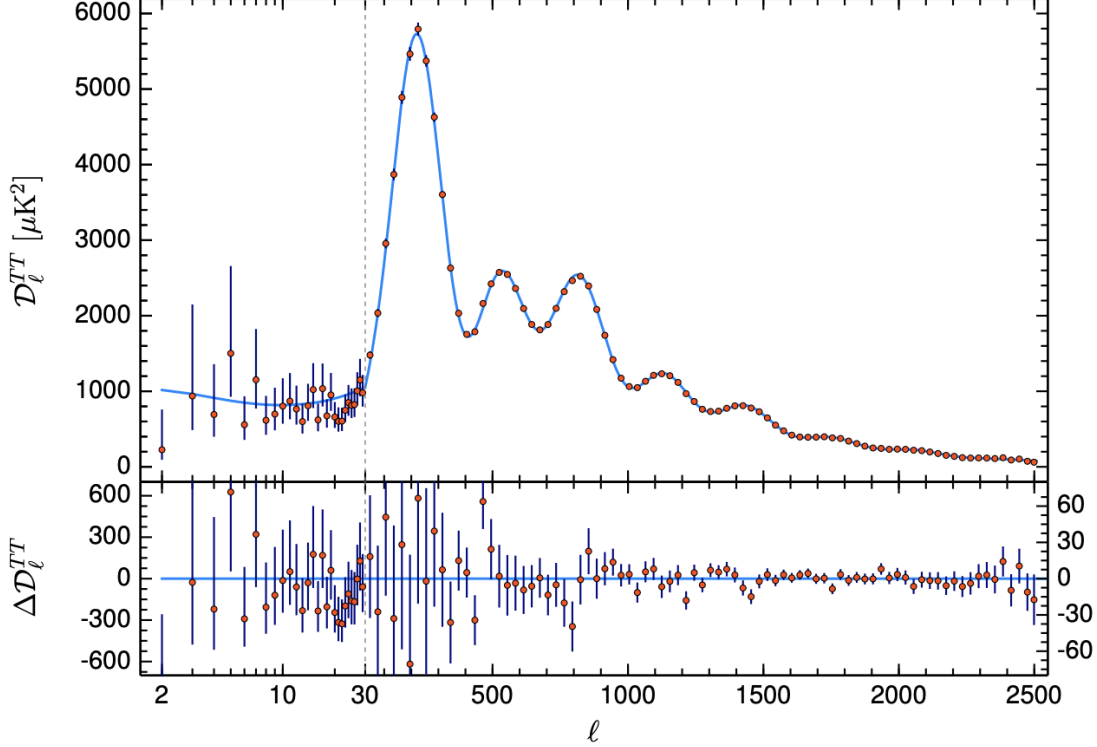


Figure 6. The angular power spectrum of the CMB. The first peak corresponds to the fundamental frequency, with the lower amplitude peaks corresponding to overtone frequencies. Source: [Aghanim et al. \(2020\)](#).

- (a) with PArthENoPE, assuming the experimental rate from [Adelberger et al. \(2011\)](#);
- (b) with PArthENoPE, using the theoretical rate of [Marcucci et al. \(2016\)](#);
- (c) with PRIMAT, using the rate from [Iliadis et al. \(2016\)](#), based on a hybrid method that consists of assuming the energy dependence of the rate computed ab initio by [Marcucci et al. \(2005\)](#) and normalizing it with a fit to a selection of laboratory measurements.

In addition to the $d(p, \gamma)^3\text{He}$ reaction rates, PArthENoPE, PRIMAT make different assumptions on other rates. When using approaches (a), (b), or (c), [Aghanim et al. \(2020\)](#) computed theoretical errors as follows. For (a), [Adelberger et al. \(2011\)](#) estimate that the error in their extrapolated rate propagates to $\sigma(y_{DP}) = 0.06$. For (b), [Aghanim et al. \(2020\)](#) rely on the claim by [Marcucci et al. \(2016\)](#) that the error is dominated by uncertainties on deuterium fusion and propagates to $\sigma(y_{DP}) = 0.03$. For (c), the error computed by PRIMAT is similar, $\sigma(y_{DP}) = 0.032$.

With the three assumptions (a), (b), and (c) on standard BBN and the determination of ω_b by *Planck* 2018 for the base- ΛCDM model, [Aghanim et al. \(2020\)](#) used Equation 71 in their work to compute:

- (a) $y = 2.587 \pm^{0.13}_{0.13}$
- (b) $y = 2.455 \pm^{0.081}_{0.080}$

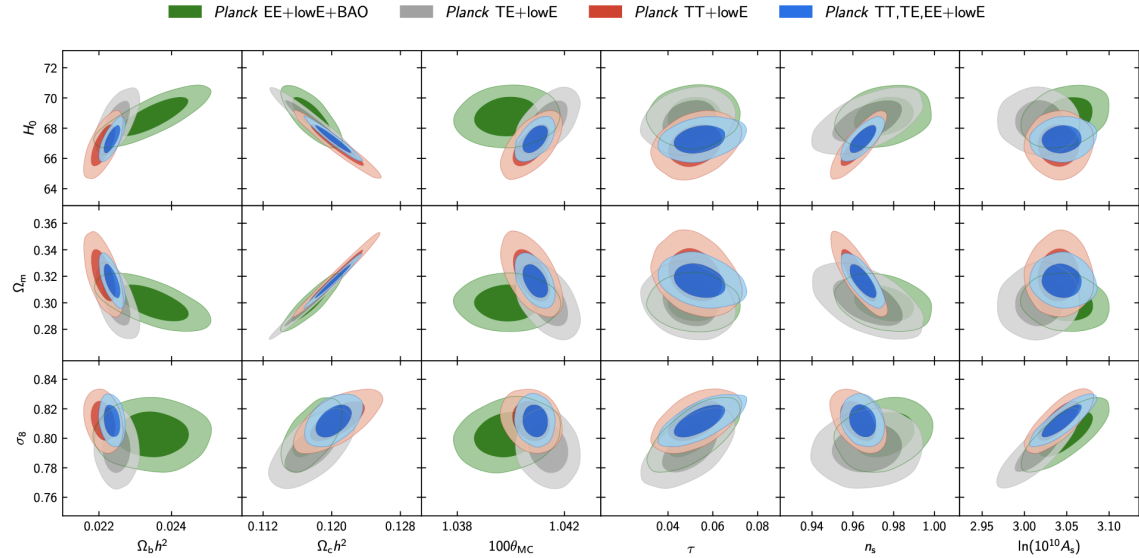


Figure 7. Constraints on parameters of the base-CDM model from the separate Planck EE, TE, and TT high- l spectra combined with low- l polarization (lowE), and, in the case of EE also with BAO (described in Sect. 5.1), compared to the joint result using Planck TT,TE,EE+lowE. Parameters on the bottom axis are our sampled MCMC parameters with flat priors, and parameters on the left axis are derived parameters (with H_0 in km s $^{-1}$ Mpc $^{-1}$). Contours contain 68 % and 95 % of the probability. Source: [Aghanim et al. \(2020\)](#)

$$(c) \quad y = 2.439 \pm^{0.082}_{0.081}$$

where the error bars include the error in ω_b and the theoretical uncertainty. The results are consistent with the [Cooke et al. \(2018\)](#) measurement to within 0.8σ , 1.4σ , and 1.7σ , respectively.

Hydrogen constitutes about 75% of all ordinary matter in the Universe. Figure 8 shows the relative abundances of solar system elements versus atomic number Z , the number of protons in the nucleus.

The primordial abundance of ^7Li inferred from observations of metal-poor stars is $^7\text{Li}/\text{H} = 1.6 \pm 0.3 \times 10^{-10}$ ([Sbordone et al. 2010](#)).

Using chemical abundance measurements and other information such as stellar parameters, coordinates, magnitudes, and radial velocities, for extremely metal-poor stars from the literature, [Abdalla & Frebel \(2018\)](#) created a database which contains 1658 unique stars, 60% of which have $[\text{Fe}/\text{H}] < 2.5$.

6. MORE BARYONIC MATTER THAN ANTIMATTER

After antimatter has been discovered ([Anderson 1932](#)), the observed excess of matter over antimatter became one of the central questions in cosmology. The baryon asymmetry of the universe (BAU) can be defined as the difference between the number of baryons N_B and antibaryons $N_{\bar{B}}$ divided by their sum just before antiprotons disappeared from the primordial plasma. Since the end products of annihilation pro-

Logarithmic SAD Abundances: Log(H) = 12.0

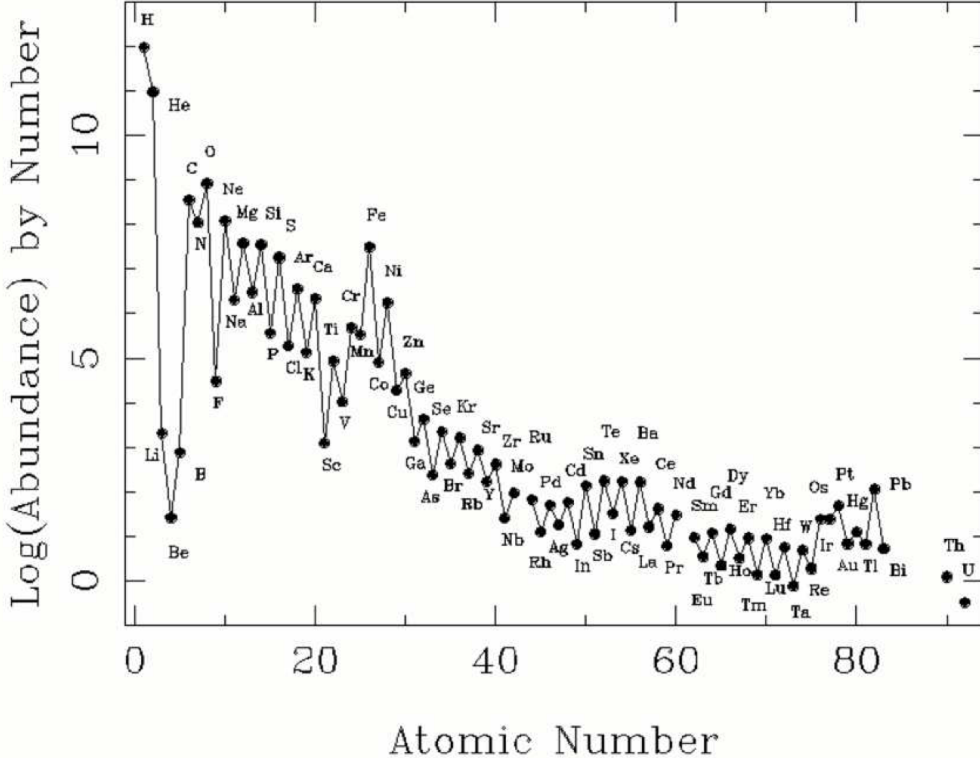


Figure 8. Solar abundances by number, i.e. vertical axis is $\log(X_Z/\bar{A}_Z) + \text{constant}$, where X_Z is the abundance of element Z by mass and \bar{A}_Z is the mean atomic weight of that element (C. R. Crowley, U Mich).

cesses are mostly photons and there are no antibaryons in the universe today, the BAU can be estimated by the baryon to photon ratio η :

$$\eta = \frac{N_B - N_{\bar{B}}}{N_\gamma} |_{3K}$$

Here the assumption is that the BAU is the same everywhere in space within the observable Universe. We can determine η independently in two ways: from the abundances of light elements in the intergalactic medium and from the power spectrum of temperature fluctuations in the Cosmic Microwave Background (Canetti et al. 2012).

Within Λ CDM and the Standard Model, η can be uniquely determined from the measurements of the primordial abundances of light elements. Steigman (2010) provides the following estimate, in units of 10^{-10} :

$$\eta_{SBBN} = 5.80 \pm 0.27.$$

We can also estimate η from the power spectrum of temperature fluctuations in the Cosmic Microwave Background. These temperature fluctuations were produced by acoustic oscillations of the baryon-photon plasma in the gravitational potential which were caused by inhomogeneities in the Dark Matter distribution (Canetti et al.

2012). The baryon fraction η determines the equation of state of the plasma, which influences the relative height of odd and even peaks in the power spectrum. The 7-year WMAP data (Komatsu et al. 2011) gives, in units of 10^{-10} :

$$\eta_{CMB} = 6.160 \pm^{0.153}_{0.156}.$$

7. HIERARCHY OF GRAVITATIONALLY BOUND STRUCTURE: BOTTOM TO TOP

The two-point correlation function $\zeta(r)$ gives the excess probability of finding a clump of matter at a certain distance r from another clump, relative to a random, Poisson-distributed matter. This allows us to describe how much the Universe clumps on the various scales. The Fourier transform of $\zeta(r)$ is the matter power spectrum $P(k)$, where $k = \frac{2\pi}{r}$ is the wavenumber. The power spectrum $P(k)$ can be written as the product of the primordial power spectrum $P_*(k)$ originating from cosmic inflation, and the square of a transfer function $T(k)$ which describes what happens at a later epoch (Peebles 1980).

Tegmark & Zaldarriaga (2002) combines measurements of the Cosmic Microwave Background, 2dF galaxies, cluster abundance, weak lensing, and Lyman Alpha Forest to compute $P(k)$ (see Figure 9). Note that $P(k)$ rises for small k , reaches a maximum and then decreases as a power-law ($P_*(k) \propto k^{n_s-1}$; Aghanim et al. (2020) used *Planck* data and estimated the scalar spectral index to be $n_s = 0.965 \pm 0.004$). The black points on Figure 9 were computed using CMB data. Anisotropies in the CMB reflect how matter clumped in the very early Universe; the polarization pattern, caused by subsequent scattering, gives constraints on matter distribution in later epochs. Green points on Figure 9 are based on data from the 2dF Galaxy Redshift survey (Colless et al. 2001), which allows to constrain how matter has formed structure on (comoving) scales from about a few tens of Mpc to several hundred Mpc. The blue points in the Figure are derived from abundances of galaxy clusters; the error bars reflect the spread in the literature. The points of magenta color are based on weak lensing data from Hoekstra et al. (2002), which uses photons from distant galaxies as test particles to measure the metric fluctuations caused by intervening matter; this technique probes the power spectrum on 10 Mpc scales. The red points are based on probes of the Lyman-alpha forest, which is a series of absorption lines in the spectra of distant galaxies and quasars arising from the Lyman-alpha electron transition of the neutral hydrogen atom (Croft et al. 2002; Gnedin & Hamilton 2002).

Each measured data point d_i shown in Figure 9 can be written as an integral $d_i = \int_{-\infty}^{\infty} P_i(k) d \ln k$ over (linear) wavenumber k for some non-negative integrand $P_i(k)$. Renormalizing $P_i(k)$ to be a probability distribution, the convention in Figure 6 is the following:

Plot the data point at the k -value corresponding to the median of this distribution with a horizontal bar ranging from the 20th to the 80th percentile.

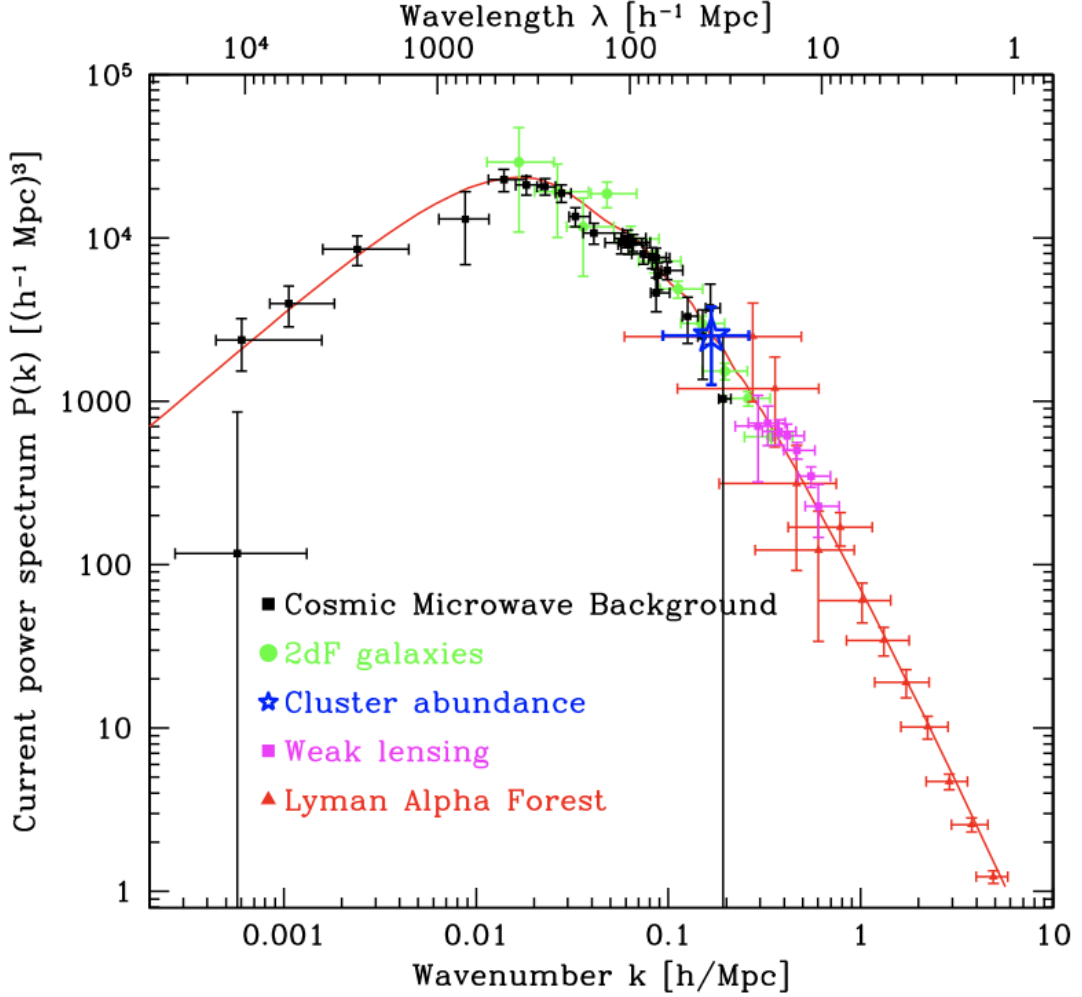


Figure 9. The matter power spectrum as a function of wavenumber. λ axis gives the corresponding spatial scale, expressed in comoving megaparsecs and divided by the dimensionless Hubble constant $h = H_0/100 \text{ km s}^{-1} \text{ Mpc}^{-1}$. Source: [Tegmark & Zaldarriaga \(2002\)](#).

Thus, the horizontal bars on the plot indicate the range of scales k contributing to the data point. All transfer functions used to produce Figure 9 assume the flat ΛCDM concordance model ([Efstathiou et al. 2002](#)).

8. ORDINARY MATTER = 1/5 ALL MATTER

The matter density in the Universe is related to the scale-dependence of the amplitude in the CMB spectra, the amount of lensing in the CMB spectra, and the amplitude of the CMB-lensing reconstruction spectrum. Using *Planck* data, [Aghanim et al. \(2020\)](#) estimates the dark matter density to be $\Omega_c h^2 = 0.120 \pm 0.001$ and the baryon density to be $\Omega_b h^2 = 0.0224 \pm 0.0001$. So the ordinary matter density is about 1/5 of the dark matter density.

9. EXISTENCE OF SUPER-MASSIVE BLACK HOLES

It has been observed that cores of many galaxies in our Universe contain a supermassive Black Hole (Kormendy & Ho 2013). The observed correlation between the stellar velocity dispersion and the mass of the core Black Hole suggests that there is a link between the evolution of massive black holes and the evolution of galaxies (Woo et al. 2019). Understanding this connection better is one of the main reasons why astronomers are interested in detecting and studying Black Holes. Let us now discuss a few recent discoveries of Super-Massive Black Holes.

Voggel et al. (2021) used the high spatial resolution mode of the integral-field spectrograph MUSE on the VLT in adaptive optics mode to resolve the stellar kinematics within the sphere of influence of two nuclei in NGC 7727. Combining the kinematic data with an HST-based mass model and using Jeans models, the authors report a significant detection of two super-massive black holes, one with a mass of $M_{SMBH} = 1.54 \pm^{0.18}_{0.15} \times 10^8 M_\odot$ and one with a mass of $M_{BH} = 6.33 \pm^{3.32}_{1.40} \times 10^6 M_\odot$.

Saracino et al. (2022) provide the first direct dynamical detection of a black hole in a young massive cluster. Using 17 epochs of Very Large Telescope/Multi-Unit Spectroscopic Explorer observations, the authors detected variations in the radial velocity associated with the target star which were exceeding 300 km s^{-1} . Assuming a semidetached system, the authors performed simultaneous modelling of radial velocity and light curves and concluded that the true mass of the unseen companion is $11.1 \pm^{2.1}_{2.4} M_\odot$.

von Fellenberg et al. (2018) report the first detection of the Galactic Centre massive black hole, Sgr A*, at $100 \mu\text{m}$ and $160 \mu\text{m}$. Using the measurements obtained with PACS on board the *Herschel* satellite, the authors measured a significant and simultaneous variation of the Galactic Center flux and provided a rigorous reasoning that supports the interpretation that this variability is caused by the presence of a massive black hole at the Galactic Center.

As understood in General Relativity, a Black hole causes gravitational light bending at its event horizon, which is theoretically predicted to produce a dark shadow when the Black hole is surrounded by a transparent emission region. The Event Horizon Telescope, a global very long baseline interferometry array observing at a wavelength of 1.3 mm was built to capture event-horizon-scale images of the supermassive black hole candidate in the center of the giant elliptical galaxy M87 (Event Horizon Telescope Collaboration et al. 2019). The authors have resolved the central compact radio source as an asymmetric bright emission ring with a diameter of $42 \pm 3 \mu\text{as}$ (see Figure 10).

10. TOTAL MASS ENERGY = 30 % OF TOTAL ENERGY

The matter density in the Universe is related to the scale-dependence of the amplitude in the CMB spectra, the amount of lensing in the CMB spectra, and the amplitude of the CMB-lensing reconstruction spectrum. In the base- Λ CDM model, Aghanim et al. (2020) used the *Planck* data to constrain the matter den-

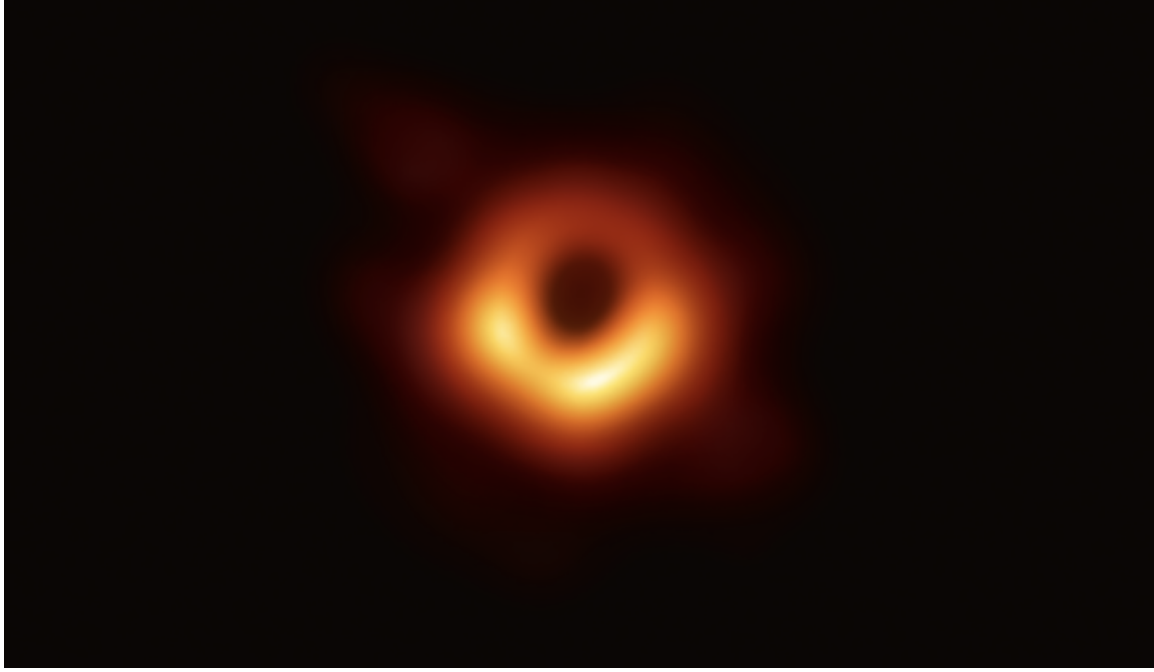


Figure 10. EHT image of M87*. For details, see Event Horizon Telescope Collaboration et al. (2019).

sity: $\Omega_m = 0.3158 \pm 0.0073$ (68 %, TT,TE,EE+lowE+lensing). Adding BAO data, the authors obtain $\Omega_m = 0.3111 \pm 0.0056$ (68 %, TT,TE,EE+lowE+lensing+BAO).

Assuming a flat universe, Aghanim et al. (2020) translate their constraint on Ω_m into a constraint on the dark-energy density parameter: $\Omega_\Lambda = 0.6847 \pm 0.0073$ (68 %, TT, TE, EE+lowE+lensing).

11. ENTROPY

It is widely believed that the second law of thermodynamics holds on the scales of the Universe: entropy only increases on average. When discussing the entropy of the Universe, it is important to consider both the radiation and matter degrees of freedom as well as the gravitational (spacetime) degrees of freedom. Classical thermodynamics fails to account for the fact that the entropy of the Universe has always been increasing at a high rate and nonetheless has not yet reached its maximum value. To address this issue, Tolman (1931) used his extension of thermodynamics to general relativity – relativistic thermodynamics – to show the possibility of thermodynamic changes which could take place at a finite rate and at the same time reversibly without increase in entropy.

Cabrera et al. (2017) provides a dynamical estimate for the Boltzmann entropy of the Universe, under the simplifying assumptions of Newtonian cosmology. The authors modeled the cosmological fluid as the probability fluid of a quantum-mechanical system and viewed gravitational equipotentials as isoentropic surfaces. Both the perturbative and the nonperturbative analysis of Cabrera et al. (2017) yielded similar

results: the estimated $\langle S_g \rangle / k_B \sim 10^{123}$ saturate the upper bound determined from the holographic principle (Bousso 2002). Some works (see e.g. Egan & Lineweaver (2010); Frampton et al. (2009)) estimate $\langle S_g \rangle / k_B$ at around 10^{104} .

At the time of CMB emergence, there was a peculiar partition of entropy: most entropy was in matter and radiation, and almost none was in gravitational field (Banks & Fischler 2021). Nowadays, almost all of the entropy in the universe is in the form of Bekenstein-Hawking (BH) entropy of super-massive black holes (Aurell et al. 2021). Peculiarities of the partition of entropy in the Universe are predicted in certain cosmological models. For example, Ijjas & Steinhardt (2022) tracked the evolution of entropy and black holes in a cyclic universe that undergoes repeated intervals of expansion followed by slow contraction and a non-singular bounce. The authors showed that the entropy problem of big bang cosmology is avoided and that the entropy following each bounce is partitioned into near-maximal entropy in the matter-radiation sector and near-minimal in the gravitational sector, which is necessary for a cosmology to be consistent with observations.

12. VACUUM MAY BE METASTABLE OR UNSTABLE

The Higgs boson was discovered by the ATLAS and CMS collaborations in 2012 (Aad et al. 2012). Figure 11 shows the distributions of the invariant mass, $m_{\gamma\gamma}$, of the diphoton events, summed over all categories, as reported in Aad et al. (2012). The red curve is a fit including a signal component with $m_H = 126.5$ GeV and a superimposed background component described by a fourth-order Bernstein polynomial. In addition, in Figure 12, we show the best-fit signal strength $\hat{\mu}$ as a function of m_H ; we see a clear peak at around $m_H = 126.5$ GeV, corresponding to the approximate mass of the Higgs boson. By using statistical analysis, Aad et al. (2012) conclude that the data are compatible with the production and decay of the Standard Model Higgs boson.

The systematic uncertainties that had the largest impact on the sensitivity of the search for the Higgs boson were the theoretical uncertainties associated with the signal. The main experimental uncertainties were associated with the JES, the jet energy resolution (JER), pile-up, E_T^{miss} , the b -tagging efficiency, the $W +$ jets transfer factor, and the integrated luminosity. The largest uncertainties on the backgrounds include $W W$ normalization and modelling, top normalization, and $W_\gamma^{(*)}$ normalization. The 2-jet systematic uncertainties are based on the statistical uncertainties in the data and the Markov Chain simulation.

More recently, the mass of the Higgs boson was measured to be $M_h = 125.18 \pm 0.16$ GeV (Tanabashi et al. 2018), which lies in a regime that predicts the metastability of the electroweak vacuum, i.e. there is a lower energy vacuum state available to which the current electroweak vacuum can decay into (Degrassi et al. 2012; Buttazzo et al. 2013). The Standard Model allows for the possibility of the current vacuum to be

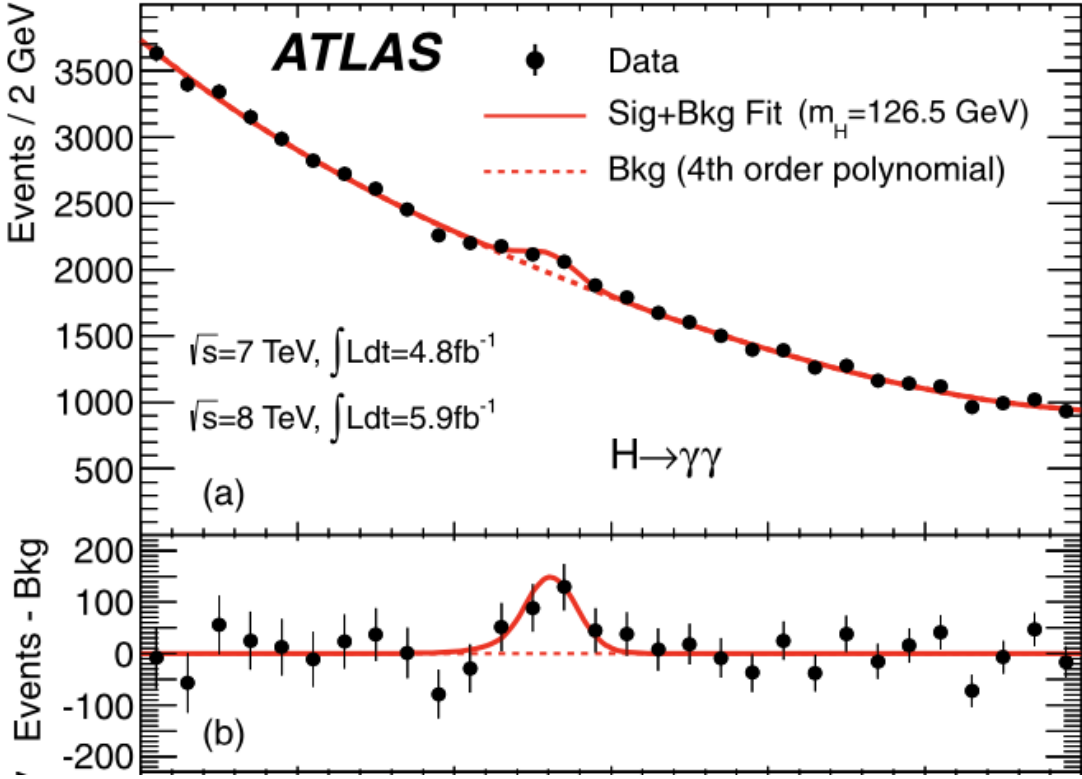


Figure 11. The distributions of the invariant mass of diphoton candidates after all selections for the combined 7 TeV and 8 TeV data sample in Aad et al. (2012). The inclusive sample is shown in the upper subplot. The red curve shows a fit including a signal component with $m_H = 126.5 \text{ GeV}$ and a superimposed background component described by a fourth-order Bernstein polynomial. The residuals of the data with respect to the fitted background are displayed in the lower subplot.

metastable (Hung 1979; Sher 1993; Casas et al. 1996; Isidori et al. 2001; Ellis et al. 2009; Elias-Miró et al. 2012).

The metastability of the Higgs vacuum has important implications in cosmology because it allows to place constraints on the cosmological history of the Universe, including the reheat temperature and the scale of inflation, and some Standard Model parameters, such as particle masses and the coupling between the Higgs field and spacetime curvature. For example, one implication is that the decay rate had to be sufficiently slow in the past for the Universe to stay in the metastable electroweak-scale state. This requires that no bubbles of true vacuum were nucleated in our past light cone because, once nucleated, a bubble of true vacuum expands at the speed of light and destroys everything in its way (Espinosa et al. 2008).

REFERENCES

- Aad, G., Abajyan, T., Abbott, B., et al. 2012, Physics Letters B, 716, 1, doi: [10.1016/j.physletb.2012.08.020](https://doi.org/10.1016/j.physletb.2012.08.020)
- Abohalima, A., & Frebel, A. 2018, The Astrophysical Journal Supplement Series, 238, 36, doi: [10.3847/1538-4365/aadfe9](https://doi.org/10.3847/1538-4365/aadfe9)

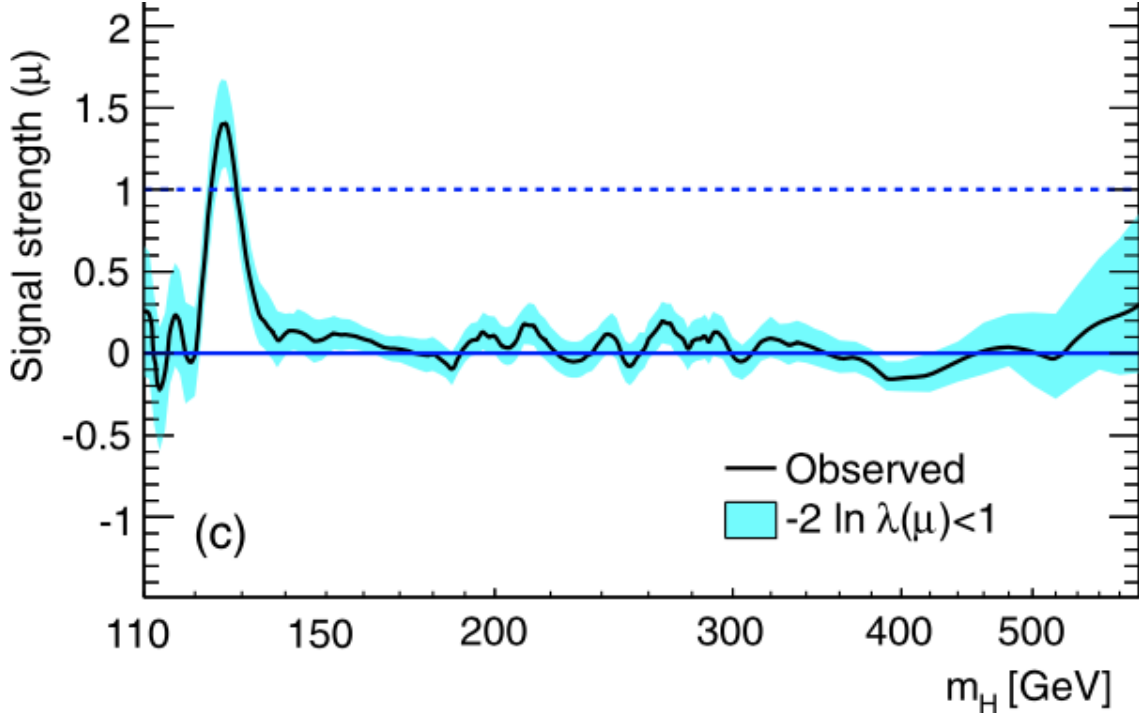


Figure 12. The best-fit signal strength $\hat{\mu}$ as a function of m_H . The blue band shows the approximate 68% CL interval around the fitted value. Source: Aad et al. (2012).

- Addison, G. E., Huang, Y., Watts, D. J., et al. 2016, *The Astrophysical Journal*, 818, 132,
doi: [10.3847/0004-637x/818/2/132](https://doi.org/10.3847/0004-637x/818/2/132)
- Adelberger, E. G., Garcí a, A., Robertson, R. G. H., et al. 2011, *Reviews of Modern Physics*, 83, 195,
doi: [10.1103/revmodphys.83.195](https://doi.org/10.1103/revmodphys.83.195)
- Aghanim, N., Akrami, Y., Ashdown, M., et al. 2020, *Astronomy & Astrophysics*, 641, A6,
doi: [10.1051/0004-6361/201833910](https://doi.org/10.1051/0004-6361/201833910)
- and N. Aghanim, Akrami, Y., Ashdown, M., et al. 2017, *Astronomy & Astrophysics*, 607, A95,
doi: [10.1051/0004-6361/201629504](https://doi.org/10.1051/0004-6361/201629504)
- Anderson, C. D. 1932, *Science*, 76, 238,
doi: [10.1126/science.76.1967.238](https://doi.org/10.1126/science.76.1967.238)
- Andrade, U., Bengaly, C. A. P., Santos, B., & Alcaniz, J. S. 2018, *ApJ*, 865, 119, doi: [10.3847/1538-4357/aadb90](https://doi.org/10.3847/1538-4357/aadb90)
- Aurell, E., Eckstein, M., & Horodecki, P. 2021, *Foundations of Physics*, 51, 54,
doi: [10.1007/s10701-021-00456-7](https://doi.org/10.1007/s10701-021-00456-7)
- Banks, T., & Fischler, W. 2021, arXiv e-prints, arXiv:2109.05571.
<https://arxiv.org/abs/2109.05571>
- Boggess, N. W., Mather, J. C., Weiss, R., et al. 1992, *ApJ*, 397, 420,
doi: [10.1086/171797](https://doi.org/10.1086/171797)
- Bousso, R. 2002, *Reviews of Modern Physics*, 74, 825–874,
doi: [10.1103/revmodphys.74.825](https://doi.org/10.1103/revmodphys.74.825)
- Buttazzo, D., Degrassi, G., Giardino, P. P., et al. 2013, *Journal of High Energy Physics*, 2013,
doi: [10.1007/jhep12\(2013\)089](https://doi.org/10.1007/jhep12(2013)089)
- Cabrera, D., Fernandez de Cordoba, P., & Isidro, J. M. 2017, arXiv e-prints, arXiv:1703.08082.
<https://arxiv.org/abs/1703.08082>
- Camarena, D., & Marra, V. 2018, *PhRvD*, 98, 023537,
doi: [10.1103/PhysRevD.98.023537](https://doi.org/10.1103/PhysRevD.98.023537)
- Canetti, L., Drewes, M., & Shaposhnikov, M. 2012, *New Journal of Physics*, 14, 095012,
doi: [10.1088/1367-2630/14/9/095012](https://doi.org/10.1088/1367-2630/14/9/095012)

- Casas, J., Espinosa, J., & Quirós, M. 1996, Physics Letters B, 382, 374, doi: [10.1016/0370-2693\(96\)00682-x](https://doi.org/10.1016/0370-2693(96)00682-x)
- Chudaykin, A., Dolgikh, K., & Ivanov, M. M. 2021, PhRvD, 103, 023507, doi: [10.1103/PhysRevD.103.023507](https://doi.org/10.1103/PhysRevD.103.023507)
- Clarkson, C., & Maartens, R. 2010, Classical and Quantum Gravity, 27, 124008, doi: [10.1088/0264-9381/27/12/124008](https://doi.org/10.1088/0264-9381/27/12/124008)
- Colless, M., Dalton, G., Maddox, S., et al. 2001, Monthly Notices of the Royal Astronomical Society, 328, 1039, doi: [10.1046/j.1365-8711.2001.04902.x](https://doi.org/10.1046/j.1365-8711.2001.04902.x)
- Cooke, R. J., Pettini, M., & Steidel, C. C. 2018, The Astrophysical Journal, 855, 102, doi: [10.3847/1538-4357/aaab53](https://doi.org/10.3847/1538-4357/aaab53)
- Croft, R. A. C., Weinberg, D. H., Bolte, M., et al. 2002, The Astrophysical Journal, 581, 20, doi: [10.1086/344099](https://doi.org/10.1086/344099)
- Degrassi, G., Vita, S. D., Elias-Miró, J., et al. 2012, Journal of High Energy Physics, 2012, doi: [10.1007/jhep08\(2012\)098](https://doi.org/10.1007/jhep08(2012)098)
- Di Valentino, E., Melchiorri, A., & Silk, J. 2021, ApJL, 908, L9, doi: [10.3847/2041-8213/abe1c4](https://doi.org/10.3847/2041-8213/abe1c4)
- Dicke, R. H., Peebles, P. J. E., Roll, P. G., & Wilkinson, D. T. 1965, ApJ, 142, 414, doi: [10.1086/148306](https://doi.org/10.1086/148306)
- Domínguez, A., Wojtak, R., Finke, J., et al. 2019, ApJ, 885, 137, doi: [10.3847/1538-4357/ab4a0e](https://doi.org/10.3847/1538-4357/ab4a0e)
- Efstathiou, G., Moody, S., Peacock, J. A., et al. 2002, MNRAS, 330, L29, doi: [10.1046/j.1365-8711.2002.05215.x](https://doi.org/10.1046/j.1365-8711.2002.05215.x)
- Egan, C. A., & Lineweaver, C. H. 2010, The Astrophysical Journal, 710, 1825–1834, doi: [10.1088/0004-637x/710/2/1825](https://doi.org/10.1088/0004-637x/710/2/1825)
- Elias-Miró, J., Espinosa, J. R., Giudice, G. F., et al. 2012, Physics Letters B, 709, 222, doi: [10.1016/j.physletb.2012.02.013](https://doi.org/10.1016/j.physletb.2012.02.013)
- Ellis, J., Espinosa, J., Giudice, G., Hoecker, A., & Riotto, A. 2009, Physics Letters B, 679, 369, doi: [10.1016/j.physletb.2009.07.054](https://doi.org/10.1016/j.physletb.2009.07.054)
- Espinosa, J. R., Giudice, G. F., & Riotto, A. 2008, Journal of Cosmology and Astroparticle Physics, 2008, 002, doi: [10.1088/1475-7516/2008/05/002](https://doi.org/10.1088/1475-7516/2008/05/002)
- Event Horizon Telescope Collaboration, Akiyama, K., Alberdi, A., et al. 2019, ApJL, 875, L1, doi: [10.3847/2041-8213/ab0ec7](https://doi.org/10.3847/2041-8213/ab0ec7)
- Fixsen, D. J., Cheng, E. S., Gales, J. M., et al. 1996, The Astrophysical Journal, 473, 576–587, doi: [10.1086/178173](https://doi.org/10.1086/178173)
- Fixsen, D. J., Hinshaw, G., Bennett, C. L., & Mather, J. C. 1997, The Astrophysical Journal, 486, 623–628, doi: [10.1086/304560](https://doi.org/10.1086/304560)
- Frampton, P. H., Hsu, S. D. H., Kephart, T. W., & Reeb, D. 2009, Classical and Quantum Gravity, 26, 145005, doi: [10.1088/0264-9381/26/14/145005](https://doi.org/10.1088/0264-9381/26/14/145005)
- Freedman, W. L., Madore, B. F., Hoyt, T., et al. 2020, ApJ, 891, 57, doi: [10.3847/1538-4357/ab7339](https://doi.org/10.3847/1538-4357/ab7339)
- Gnedin, N. Y., & Hamilton, A. J. S. 2002, MNRAS, 334, 107, doi: [10.1046/j.1365-8711.2002.05490.x](https://doi.org/10.1046/j.1365-8711.2002.05490.x)
- Gonçalves, R. S., Carvalho, G. C., Bengaly, C. A. P., J., et al. 2018, MNRAS, 475, L20, doi: [10.1093/mnrasl/slx202](https://doi.org/10.1093/mnrasl/slx202)
- Goodman, J. 1995, PhRvD, 52, 1821, doi: [10.1103/PhysRevD.52.1821](https://doi.org/10.1103/PhysRevD.52.1821)
- Hagstotz, S., Reischke, R., & Lilow, R. 2022, MNRAS, 511, 662, doi: [10.1093/mnras/stac077](https://doi.org/10.1093/mnras/stac077)
- Hoekstra, H., Yee, H. K. C., & Gladders, M. D. 2002, The Astrophysical Journal, 577, 595, doi: [10.1086/342120](https://doi.org/10.1086/342120)
- Hu, W., & White, M. 2004, Scientific American, 290, 44, doi: [10.1038/scientificamerican0204-44](https://doi.org/10.1038/scientificamerican0204-44)
- Hubble, E. 1929, Proceedings of the National Academy of Sciences, 15, 168, doi: [10.1073/pnas.15.3.168](https://doi.org/10.1073/pnas.15.3.168)
- Hung, P. Q. 1979, Physical Review Letters, 42, 873, doi: [10.1103/physrevlett.42.873](https://doi.org/10.1103/physrevlett.42.873)
- Ijjas, A., & Steinhardt, P. J. 2022, Physics Letters B, 824, 136823, doi: [10.1016/j.physletb.2021.136823](https://doi.org/10.1016/j.physletb.2021.136823)

- Iliadis, C., Anderson, K. S., Coc, A., Timmes, F. X., & Starrfield, S. 2016, *The Astrophysical Journal*, 831, 107, doi: [10.3847/0004-637x/831/1/107](https://doi.org/10.3847/0004-637x/831/1/107)
- Isidori, G., Ridolfi, G., & Strumia, A. 2001, *Nuclear Physics B*, 609, 387, doi: [10.1016/s0550-3213\(01\)00302-9](https://doi.org/10.1016/s0550-3213(01)00302-9)
- Izotov, Y. I., Thuan, T. X., & Stasińska, G. 2007, *ApJ*, 662, 15, doi: [10.1086/513601](https://doi.org/10.1086/513601)
- Khetan, N., Izzo, L., Branchesi, M., et al. 2021, *A&A*, 647, A72, doi: [10.1051/0004-6361/202039196](https://doi.org/10.1051/0004-6361/202039196)
- Komatsu, E., Smith, K. M., Dunkley, J., et al. 2011, *The Astrophysical Journal Supplement Series*, 192, 18, doi: [10.1088/0067-0049/192/2/18](https://doi.org/10.1088/0067-0049/192/2/18)
- Kormendy, J., & Ho, L. C. 2013, *Annual Review of Astronomy and Astrophysics*, 51, 511, doi: [10.1146/annurev-astro-082708-101811](https://doi.org/10.1146/annurev-astro-082708-101811)
- Kurichin, O. A., Kislytsyn, P. A., Klimenko, V. V., Balashev, S. A., & Ivanchik, A. V. 2021, *Monthly Notices of the Royal Astronomical Society*, 502, 3045, doi: [10.1093/mnras/stab215](https://doi.org/10.1093/mnras/stab215)
- Marcucci, L., Mangano, G., Kievsky, A., & Viviani, M. 2016, *Physical Review Letters*, 116, doi: [10.1103/physrevlett.116.102501](https://doi.org/10.1103/physrevlett.116.102501)
- Marcucci, L., Viviani, M., Schiavilla, R., Kievsky, A., & Rosati, S. 2005, *Physical Review C*, 72, doi: [10.1103/physrevc.72.014001](https://doi.org/10.1103/physrevc.72.014001)
- Ntelis, P., Hamilton, J.-C., Le Goff, J.-M., et al. 2017, *JCAP*, 2017, 019, doi: [10.1088/1475-7516/2017/06/019](https://doi.org/10.1088/1475-7516/2017/06/019)
- Peebles, P. J. E. 1980, *The large-scale structure of the universe*
- Penzias, A. A., & Wilson, R. W. 1965, *ApJ*, 142, 419, doi: [10.1086/148307](https://doi.org/10.1086/148307)
- Planck Collaboration, Ade, P. A. R., Aghanim, N., et al. 2016, *A&A*, 594, A13, doi: [10.1051/0004-6361/201525830](https://doi.org/10.1051/0004-6361/201525830)
- Riess, A. G., Casertano, S., Yuan, W., Macri, L. M., & Scolnic, D. 2019, *The Astrophysical Journal*, 876, 85, doi: [10.3847/1538-4357/ab1422](https://doi.org/10.3847/1538-4357/ab1422)
- Riess, A. G., Casertano, S., Yuan, W., Macri, L. M., & Scolnic, D. 2019, *ApJ*, 876, 85, doi: [10.3847/1538-4357/ab1422](https://doi.org/10.3847/1538-4357/ab1422)
- Riess, A. G., Macri, L., Casertano, S., et al. 2011, *The Astrophysical Journal*, 730, 119, doi: [10.1088/0004-637x/730/2/119](https://doi.org/10.1088/0004-637x/730/2/119)
- Riess, A. G., Casertano, S., Yuan, W., et al. 2018, *The Astrophysical Journal*, 855, 136, doi: [10.3847/1538-4357/aaadb7](https://doi.org/10.3847/1538-4357/aaadb7)
- Saracino, S., Kamann, S., Guarcello, M. G., et al. 2022, *MNRAS*, 511, 2914, doi: [10.1093/mnras/stab3159](https://doi.org/10.1093/mnras/stab3159)
- Sbordone, L., Bonifacio, P., Caffau, E., et al. 2010, *A&A*, 522, A26, doi: [10.1051/0004-6361/200913282](https://doi.org/10.1051/0004-6361/200913282)
- Scolnic, D. M., Jones, D. O., Rest, A., et al. 2018, *ApJ*, 859, 101, doi: [10.3847/1538-4357/aab9bb](https://doi.org/10.3847/1538-4357/aab9bb)
- Sher, M. 1993, *Physics Letters B*, 317, 159, doi: [10.1016/0370-2693\(93\)91586-c](https://doi.org/10.1016/0370-2693(93)91586-c)
- Spergel, D. N., Flauger, R., & Hložek, R. 2015, *Physical Review D*, 91, doi: [10.1103/physrevd.91.023518](https://doi.org/10.1103/physrevd.91.023518)
- Steigman, G. 2010, *Primordial Nucleosynthesis: The Predicted and Observed Abundances and Their Consequences*, arXiv, doi: [10.48550/ARXIV.1008.4765](https://doi.org/10.48550/ARXIV.1008.4765)
- Tanabashi, M., Hagiwara, K., Hikasa, K., et al. 2018, *Phys. Rev. D*, 98, 030001, doi: [10.1103/PhysRevD.98.030001](https://doi.org/10.1103/PhysRevD.98.030001)
- Tayler, R. J. 1967, *QJRAS*, 8, 313
- Tegmark, M., & Zaldarriaga, M. 2002, *Physical Review D*, 66, doi: [10.1103/physrevd.66.103508](https://doi.org/10.1103/physrevd.66.103508)
- Tolman, R. C. 1931, *Physical Review*, 37, 1639, doi: [10.1103/PhysRev.37.1639](https://doi.org/10.1103/PhysRev.37.1639)
- Vagnozzi, S., Loeb, A., & Moresco, M. 2021, *The Astrophysical Journal*, 908, 84, doi: [10.3847/1538-4357/abd4df](https://doi.org/10.3847/1538-4357/abd4df)
- Visser, M. 2004, *Classical and Quantum Gravity*, 21, 2603, doi: [10.1088/0264-9381/21/11/006](https://doi.org/10.1088/0264-9381/21/11/006)
- Voggel, K. T., Seth, A. C., Baumgardt, H., et al. 2021, arXiv e-prints, arXiv:2111.14854. <https://arxiv.org/abs/2111.14854>

von Fellenberg, S. D., Gillessen, S.,
Graciá-Carpio, J., et al. 2018, The
Astrophysical Journal, 862, 129,
doi: [10.3847/1538-4357/aacd4b](https://doi.org/10.3847/1538-4357/aacd4b)

Woo, J.-H., Cho, H., Gallo, E., et al.
2019, Nature Astronomy, 3, 755,
doi: [10.1038/s41550-019-0790-3](https://doi.org/10.1038/s41550-019-0790-3)